

Article

Charging Characteristics of Lithium Ion Battery Using Semi-Solar Modules of Polymer:Fullerene Solar Cells

Myeonghun Song¹, Sooyong Lee¹, Dohan Kim¹, Chulyeon Lee¹, Jaehoon Jeong¹,
Jooyeok Seo¹, Hwajeong Kim^{1,2,*}, Dong-Ik Song³, Donghyun Kim⁴ and Youngkyoo Kim^{1,*}

¹ Organic Nanoelectronics Laboratory and KNU Institute for Nanophotonics Applications (KINPA), Department of Chemical Engineering, School of Applied Chemical Engineering, Kyungpook National University, University Road 80, Daegu 41566, Korea; msong@knu.ac.kr (M.S.); tomly@naver.com (S.L.); dohan278@naver.com (D.K.); lcyyeon@naver.com (C.L.); jh-jeong@knu.ac.kr (J.J.); ironmask0601@nate.com (J.S.)

² Priority Research Center, Research Institute of Advanced Energy Technology, Kyungpook National University, University Road 80, Daegu 41566, Korea

³ Polymer Rheology Laboratory, Department of Chemical Engineering, School of Applied Chemical Engineering, Kyungpook National University, University Road 80, Daegu 41566, Korea; disong@knu.ac.kr

⁴ Department of Chemical Engineering, Kyungpook National University, University Road 80, Daegu 41566, Korea; dhkim@knu.ac.kr

* Correspondence: khj217@knu.ac.kr (H.K.); ykimm@knu.ac.kr (Y.K.); Tel.: +82-053-950-5616 (H.K. & Y.K.)

Received: 24 October 2017; Accepted: 8 November 2017; Published: 16 November 2017

Abstract: The combination of lithium ion battery (LIB) and organic (polymer) solar cells is expected to deliver versatile self-rechargeable portable energy sources, but less attention has been paid to the charging characteristics of LIB-using polymer solar cells. Here we demonstrate that the LIB packs, which were prepared by using lithium cobalt oxide (LiCoO₂) and graphite as a cathode and an anode, respectively, can be effectively charged by semi-solar modules of polymer:fullerene solar cells, of which bulk heterojunction (BHJ) layers are composed of poly(3-hexylthiophene) (P3HT) and [6,6]-phenyl-C₆₁-butyric acid methyl ester (PC₆₁BM). Results showed that the performance of semi-solar modules was not much degraded by connecting four single solar cells in series or in parallel, but their output power density was noticeably reduced by extending the number of single cells up to eight. The charging test disclosed that the output current density is of importance to speed up the LIB charging at the same output voltage.

Keywords: organic solar cells; polymer:fullerene bulk heterojunctions; semi-solar modules; lithium-ion battery (LIB); charging characteristics

1. Introduction

Organic solar cells based on conjugated polymers, so called polymer solar cells (PSCs), have been extensively studied because of their capability for ultrathin and flexible plastic solar modules that can be rolled so as to secure high mobility [1–7]. Further advantages of PSCs include low-cost manufacturing by employing roll-to-roll processes using large-area plastic film substrates at low temperatures [4–9]. In terms of material constructions for active layers in PSCs, bulk heterojunction (BHJ) structures have been widely used from the early works due to their huge potential for efficient charge generation and separation processes by the tremendous number of *p-n* junctions in bulk films [10–19]. The BHJ structures can be made by mixing electron-donating (*p*-type) conjugated polymers and electron-accepting materials such as polymers, small molecules, inorganic nanoparticles, etc. [20–24].

To date, most research on PSCs has been focused on the enhancement of power conversion efficiency (PCE), while device stability has recently attracted keen interest because the PCE has been

encouragingly improved up to >10% [25–40]. In order to examine the potential of PSCs, however, practical approaches to utilizing PSCs are of crucial importance for further improvement. Since PSCs represent a type of energy conversion device from solar energy (photons) to electrical energy (electrons), it is important to understand how PSCs can sufficiently and stably deliver electricity to electrical devices (loads) including rechargeable batteries [41,42].

However, less attention has been paid to in situ charging processes for lithium ion batteries (LIBs) using PSCs, even though the pairing of solar cells and rechargeable batteries is considered the first step toward practical applications [43–45]. Taking into account the specifications of LIBs, the minimum voltage required is about >3.7 V (nominal voltage), which cannot be afforded by single PSCs. Therefore, single PSCs need to be integrated to modules via either series and/or parallel connections. A couple of solar cell modules have been reported, but actual charging experiments with LIBs have not yet been demonstrated [46–48].

In this work, we demonstrate that single LIB packs can be stably charged with the semi-solar modules of PSCs that exhibit ca. 3.5% PCE. The PSCs were fabricated with a device geometry of normal-type structure using BHJ layers of poly(3-hexylthiophene) (P3HT) and [6,6]-phenyl-C₆₁-butyric acid methyl ester (PC₆₁BM), while the LIB packs were fabricated using lithium hexafluorophosphate (LiPF₆) as an electrolyte and lithium-cobalt oxide (LiCoO₂) as a cathode. To meet the specifications of the LIBs fabricated, both series and parallel connections in the semi-solar modules were applied using 24 PSCs. Results showed that the LIB packs fabricated in this work could be quickly charged by employing hybrid configurations of both series and parallel connections of 24 PSCs compared to only series connections with the same output voltage.

2. Results

As shown in Figure 1a, the present P3HT:PC₆₁BM solar cells were fabricated by employing the well-known normal-type device structure that consists of poly(3,4-ethylenedioxythiophene):polystyrene sulfonate (PEDOT:PSS) and lithium fluoride (LiF) as a hole-collecting buffer layer (or hole-transporting layer) and an electron-collecting buffer layer (or electron-transporting layer), respectively (see the flat energy band diagram in Figure 1b). The dark current density–voltage (J–V) curve indicates that the present devices exhibit typical diode performances as expected from the flat energy band diagram in Figure 1b. Upon illumination with the simulated solar light (air mass 1.5 G, 100 mW/cm²), the J–V curve was clearly shifted down to the negative current direction leading to the generation of photocurrent (see Figure 1c). The short circuit current density (J_{SC}) of devices was 11.65 mA/cm², while the open circuit voltage (V_{OC}) reached 0.58 V. All PSCs fabricated in this study showed well-controlled PCEs between 3.3% and 3.7% (average PCE = 3.5%).

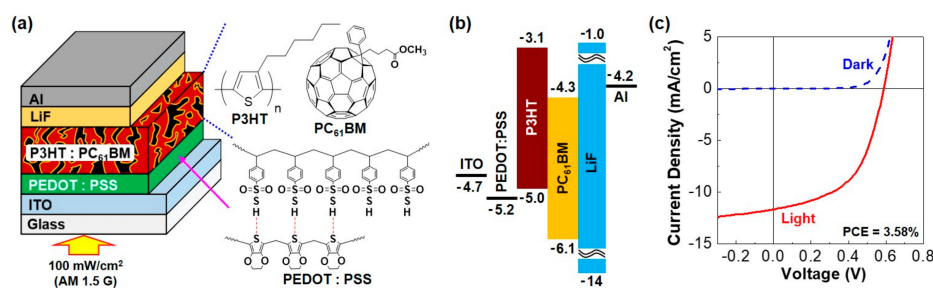


Figure 1. Device structure and performance of single P3HT:PC₆₁BM solar cells: (a) Normal-type device structure and materials used in this work; (b) Flat energy band diagram (note that the ‘eV’ unit is omitted); (c) Current density—voltage (J–V) characteristics of single P3HT:PC₆₁BM solar cells.

In order to examine the performance of semi-solar modules, four single P3HT:PC₆₁BM solar cells were connected as illustrated in Figure 2. In the case of series connection (Figure 2a left),

the indium-tin oxide (ITO) electrodes were directly connected to the aluminum (Al) electrodes. The semi-solar modules with series connection of four single P3HT:PC₆₁BM solar cells showed 2.32 V and 12.61 mA/cm² (see Figure 2a right). This result indicates that the series connection can deliver a theoretical V_{OC} value without any J_{SC} loss in the presence of marginal fill factor (FF) reduction. After the parallel connection of four single P3HT:PC₆₁BM solar cells, the J_{SC} value was measured as 46.96 mA/cm² from the semi-solar modules (see Figure 1b). This J_{SC} value is marginally lower, by 0.36 mA/cm², than the theoretical value (46.6 mA/cm²), while the V_{OC} value was measured exactly the same as expected (see Table 1). Hence, it is concluded that the present P3HT:PC₆₁BM solar cells can provide good performances close to the theoretical levels even after making semi-solar modules.

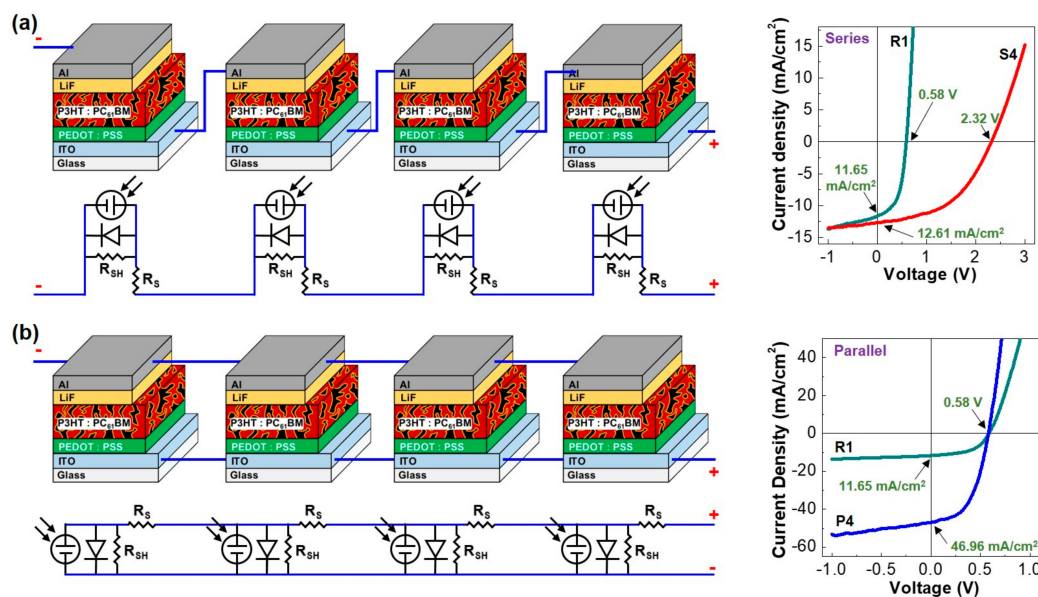


Figure 2. Semi-solar modules by series and parallel connections of single P3HT:PC₆₁BM solar cells (R1): (a) Series connection of four single cells (S4, left top), simple equivalent diagram for series connection (left bottom), and light J-V curves (right); (b) Parallel connection of four single cells (P4, left top), simple equivalent diagram for parallel connection (left bottom), and light J-V curves (right).

Table 1. Performance summary of single solar cell (R1) and two semi-solar modules of four single cells in series (S4) and parallel (P4). Note that more than 20 cells and semi-modules were tested.

Parameters	Single Cell (R1)	Four Cells in Series (S4)	Four Cells in Parallel (P4)
V _{OC} (V)	0.58 (±0.01)	2.32 (±0.02)	0.58 (±0.02)
J _{SC} (mA/cm ²)	11.65 (±0.35)	12.61 (±0.29)	46.96 (±0.32)
FF (%)	52.9 (±2.12)	48.1 (±2.31)	51.1 (±1.94)
PCE (%)	3.58 (±0.21)	3.52 (±0.19)	3.48 (±0.22)

The performance of semi-solar modules is compared according to the connection type in Figure 3. As shown in Figure 3a, the semi-solar modules with series (S4) and parallel (P4) connections have strong advantages in terms of voltage and current, respectively. Interestingly, however, the maximum power density ($P_{MM} = FF \cdot J_{SC} \cdot V_{OC}$) measured was quite similar between series and parallel connections even though it is achieved at different voltages (see Figure 3b). As summarized in Table 2, the theoretical maximum power density (P_{MT}) was calculated to be 14.32 mW/cm² for S4 and P4 by using the P_{MM} value of a single cell (R1). The deviation between P_{MM} and P_{MT} was only 2.3% and 3.2% for S4 and P4, respectively. This small deviation implies that the electrical characteristics of the present solar cells cannot be significantly affected by connecting individual cells in series or parallel.

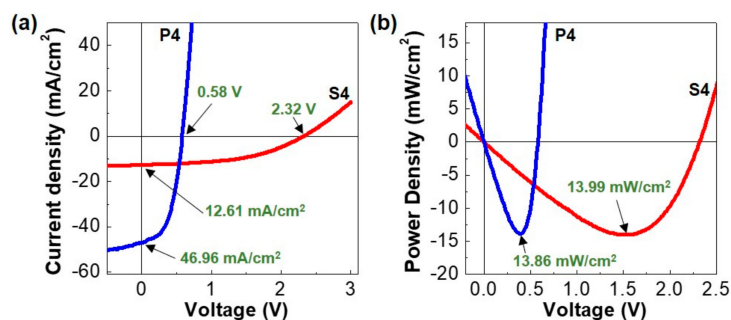


Figure 3. Comparison of semi-solar modules according to the connection type: (a) Light J-V characteristics for the semi-solar modules with series (S4) and parallel (P4) connections of four single cells; (b) Power density as a function of voltage for the semi-solar modules in (a) (see the maximum power density (P_{MM}) values indicated by the black arrows).

Table 2. Summary of power density for single solar cell (R1) and two semi-solar modules of four single cells in series (S4) and parallel (P4). The deviation (D_{MP}) between the measured (P_{MM}) and theoretical (P_{MT}) maximum power densities is given on the bottom.

Parameters	Single Cell (R1)	Four Cells in Series (S4)	Four Cells in Parallel (P4)
P_{MM} (mW/cm ²)	3.58 (± 0.17)	13.99 (± 0.27)	13.86 (± 0.31)
P_{MT} (mW/cm ²)	3.58	14.32	14.32
D_{MP} (%)	-	2.3	3.2

To examine the charging performance of semi-solar modules based on the P3HT:PC₆₁BM solar cells, lithium ion battery (LIB) packs were fabricated using graphite and lithium-cobalt oxide (LiCoO₂) as an anode and a cathode, respectively (see Figure 4a). As shown in Figure 4b, the present LIB packs showed typical charging behavior of LIBs, indicative of faster charging at a higher charging rate. Here it is noted that the measured capacity of the present LIB was ca. 1.1 mAh (see Figure 4b) at 1 C-rate, even though the theoretical capacity of LIB is up to ca. 8 mAh when it comes to the gravimetric energy density of LiCoO₂ (137 mA/g) and graphite (372 mA/g) used in this work. The reason for this can be attributable mainly to the fact that a constant current mode was applied without a mixed mode applying voltage for sufficient time for ions to move from cathode to anode. In any case, the present LIB packs, after charging, had enough capacity to turn on inorganic light-emitting devices (LEDs) (see Figure 4c).

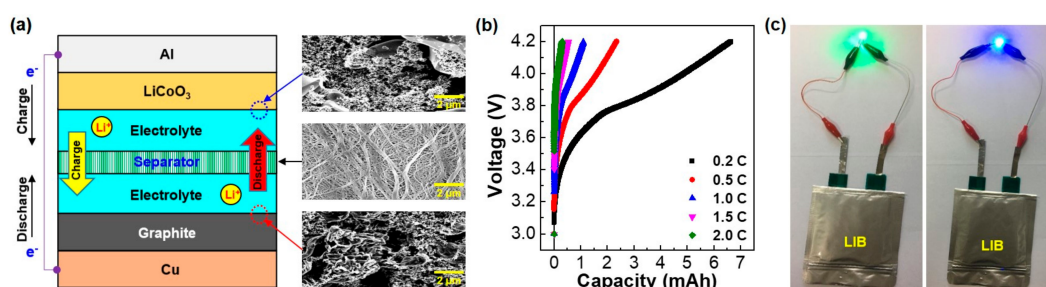


Figure 4. Device structure and performance of a lithium ion battery (LIB) fabricated in this work: (a) Schematic illustration for the cross-sectional structure of the LIB and SEM images for core materials (LiCoO₂, separator, and graphite layers); (b) Voltage-capacity characteristics according to the charging rate (0.2 C~2.0 C); (c) Photographs for the operation of light-emitting devices (LEDs) (green and blue) using the LIBs fabricated in this work.

In order to meet the minimum charging voltage (3.7 V) for the present LIB packs, an extended semi-solar module with eight single P3HT:PC₆₁BM solar cells was fabricated by series connection, leading to S8, as marked with the dotted line in Figure 5a. In order to increase the output current, three S8 semi-solar modules were further connected in parallel (see the whole diagram in Figure 5a), which is called S8_3P here. As shown in Figure 5b, the same V_{OC} (4.54 V) was measured for both S8 and S8_3P, while the J_{SC} value of S8_3P became almost triple compared to S8. As shown in Figure 5c, S8_3P exhibited almost 2.9 times higher maximum power density compared to S8.

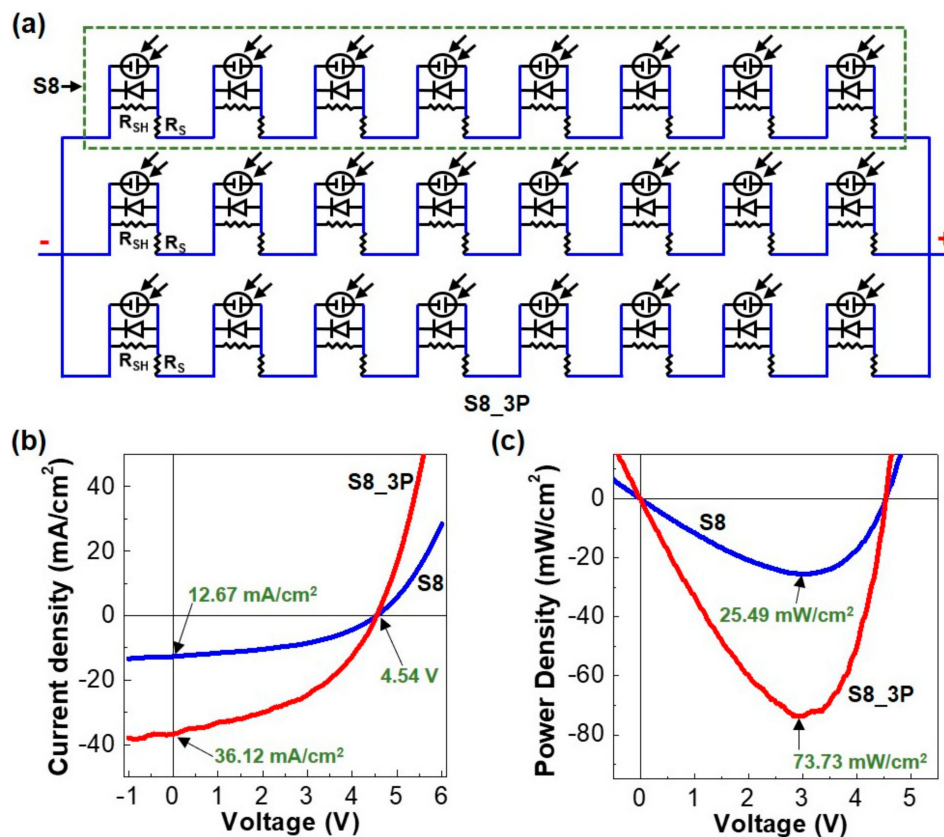


Figure 5. Extended semi-solar modules by series and parallel connections of single P3HT:PC₆₁BM solar cells: (a) Simple equivalent circuit diagram for the connection of eight single cells in series (S8) and the parallel connection of three S8 blocks leading to S8_3P; (b) Light J-V characteristics for the extended semi-solar modules; (c) Power density as a function of voltage for the extended semi-solar modules in (b) (see the maximum power density values indicated by the black arrows).

This result shows that the parallel connection of S8 did not cause a critical problem in terms of electrical characteristics. However, as shown in Table 3, the fill factor (FF) value was relatively lower for S8 and S8_3P than R1 (single cell) (see Table 1), which can be attributed to the slightly increased contact resistances. As a result, the measured maximum power density of S8 and S8_3P was relatively lower than the theoretical value, as summarized in Table 3. Considering the deviation in maximum power density for S8 and S8_3P, both series and parallel connections can gradually degrade the performance of semi-solar modules because the extended connections can give rise to the increased electrical resistances among cells and/or modules.

Table 3. Summary of power density for the extended semi-solar modules of eight single cells in series (S8) and three blocks of S8 in parallel (S8_3P). The deviation (D_{MP}) between the measured (P_{MM}) and theoretical (P_{MT}) maximum power densities is given on the bottom. Note that more than five semi-modules were tested for each case.

Parameters	S8 (Eight Cells)	S8_3P (24 Cells)
Voc (V)	4.54 (± 0.03)	4.54 (± 0.03)
Jsc (mA/cm ²)	12.67 (± 0.38)	36.12 (± 0.44)
FF (%)	44.3 (± 2.31)	46.6 (± 2.19)
PCE (%)	3.19 (± 0.29)	3.06 (± 0.32)
P_{MM} (mW/cm ²)	25.49 (± 0.42)	73.73 (± 0.44)
P_{MT} (mW/cm ²)	28.64	85.92
D_{MP} (%)	11.0	14.2

Next, the extended semi-solar modules were exposed to one sun condition (100 mW/cm²) from the solar simulator in order to charge the LIB packs fabricated in this work. As shown in Figure 6a, the LIB packs could be successfully charged using the extended semi-solar modules. The voltage of the LIB packs was increased from 3.0 V to 4.2 V by charging with the extended semi-solar modules. In more detail, however, the charging time was significantly reduced from ca. 2700 s to 340 s as the output current density was increased from 12.67 mA/cm² to 36.12 mA/cm² in the presence of the same output voltage. This result indicates that the output voltage from the extended semi-solar modules is enough to perform the basic charging process, while the output current density is a key factor. The C-rate, which is obtained from the charging time and the current density from the extended semi-solar modules, was 1.24 and 3.74, respectively.

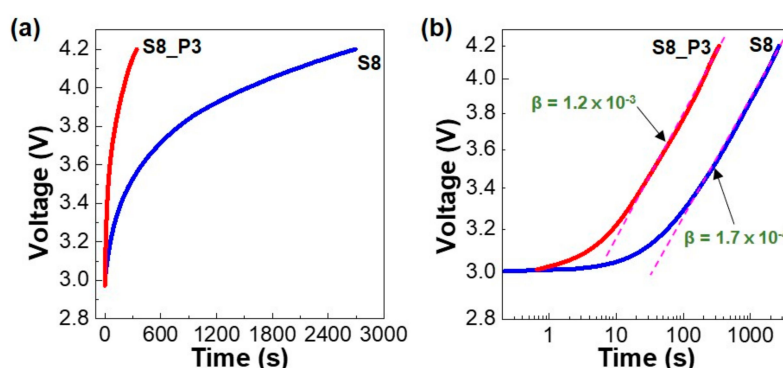


Figure 6. Charging characteristics of the fabricated LIB packs by using the extended semi-solar modules (S8 and S8_3P) under one sun condition (100 mW/cm²): (a) Voltage-time (V-t) characteristics on a linear scale; (b) Voltage-time (V-t) characteristics on a full logarithmic scale (see the charging rate constant values obtained by applying the power law equation, $V = \alpha \cdot t^\beta$, as indicated by the black arrows).

To briefly check the charging rate constant (β), a power-law equation ($V = \alpha \cdot t^\beta$ where α and t are the proportional constant and the charging time, respectively) was employed for the voltage-time plots on a full logarithmic scale under a stable charging regime (linear range). As shown in Figure 6b, the charging rate constant was 1.7×10^{-4} and 1.2×10^{-3} for S8 and S8_3P, respectively. This result reveals that the charging rate constant can be improved as high as 10-fold by making triple times the output current density through parallel connections of three S3 semi-solar modules.

3. Materials and Methods

Materials and Solution: P3HT (SOL4106, typical molecular weight = 50~70 kDa, polydispersity index = 1.4~1.6, regioregularity = 93~95%) and PC₆₁BM were purchased from Solaris (Saint-Lazare, QC, Canada) and Nano-C (Westwood, CA, USA). The PEDOT:PSS solution (PH1000) was supplied from

Clevios (Hanau, Germany) and used for hole-collecting buffer layers. The P3HT and PC₆₁BM powders were dissolved at a solid concentration of 24 mg/mL in chlorobenzene (1:1 by weight), which were subjected to vigorous stirring on a magnetic stirring plate at 60 °C before spin-coating. The cathode active materials were prepared by mixing LiCoO₂ (KD-10, Umicore, Cheonan, Korea), carbon black (Super-P Li, TIMCAL, Bodio, Switzerland) and poly(vinylidene fluoride) (PVDF) (Kureha Chemical: Tokyo, Japan). The anode active materials were prepared by mixing graphite (SCMG-AR, SHOWA DENKO, Tokyo, Japan), Super-P, and PVDF. LiPF₆ was purchased from Soulbrain (Seongnam, Korea) and used for the preparation of electrolyte solution by using ethylene carbonate (EC), ethyl methyl carbonate (EMC), dimethyl carbonate (DMC), and vinylene carbonate (VC).

PSC Fabrication: The ITO-coated glass substrates were patterned to have an ITO stripe by employing typical lithography/etching processes. The patterned ITO-glass substrates were cleaned using acetone and isopropyl alcohol for 30 min in an ultrasonic bath, followed by drying with a nitrogen flow. After cleaning and drying, the ITO-glass substrates were treated under UV-ozone for 20 min in order to remove residues. The PEDOT:PSS layers were spin-coated on the cleaned ITO-glass substrates at 2500 rpm for 60 s (thickness = 50 nm) and annealed at 230 °C for 15 min [49]. Next, the P3HT:PC₆₁BM BHJ layers (thickness = 60 nm) were spin-coated on top of the PEDOT:PSS layers at 1500 rpm for 30 s and annealed at 70 °C for 15 min. After soft-baking, all samples were transferred into a vacuum chamber inside an argon-filled glove box. LiF (~1 nm) and Al (~80 nm) were consecutively deposited on the BHJ layers through a shadow mask (active area = 0.09 cm²) at a base pressure of 1 × 10⁻⁶ Torr. Next, all devices were thermally annealed at 140 °C for 30 min.

LIB Fabrication: The active (cathode and anode) materials were mixed and stirred in a mortar in order to crush the crowded particles by adding N-methyl pyrrolidinone (NMP). Next, the anode (thickness = 150 μm) and cathode (thickness = 100 μm) active layers were coated by using a doctor blade on copper and aluminum foils, respectively. After coating, the coated electrodes were transferred and dried in a furnace at 200 °C for 24 h. Next, the dried anode and cathode samples were cut into dimensions of 4 × 4 cm² and 3 × 3 cm², respectively. Then, the separators were sandwiched between the anode and cathode foils in order to prevent any direct contact between electrodes and wrapped up electrodes. The wrapped cells were rolled at 70 °C for packing between the two electrodes and separators. Next, the rolled cells were inserted into a prepared aluminum pouch and suitably filled with the LiPF₆ electrolytes. Finally, the electrolyte-injected lithium ion battery (LIB) cells (packs) were welded using a welding machine.

Measurements and Analysis: OSC devices and modules were measured under one sun condition (100 mW/cm², air mass 1.5 G) using a solar simulator (92250A-1000, Newport-Oriel, Irvine, CA, USA) and an electrometer (Model 2400, Keithley, Cleveland, OH, USA). The characteristics of LIB were measured using a potentiostat (VersaSTAT 4, AMETEK, Berwyn, IL, USA) by varying the charging rate from 0.2 to 2 C-rate. The LIB electrodes and separator films were analyzed using a scanning electron microscope (SEM, JSM-6701F, JEOL, Tokyo, Japan). The charging characteristics of LIB by the semi-solar modules were measured using a specialized measurement system equipped with a nanovoltmeter (2182A, Keithley, Cleveland, OH, USA).

4. Conclusions

The semi-solar modules were fabricated by series and parallel connections of single P3HT:PC₆₁BM solar cells and applied for charging a lithium ion battery under continuous solar light illumination. When four single cells were connected in series, the open circuit voltage was almost the same as each cell. However, the open circuit voltage was slightly lowered by extending the number of single cells up to eight. The short circuit current density was well maintained, even after connecting eight single cells in series. The deviation in the maximum power density was noticeably increased by extending the number of single cells from four to eight. In particular, the deviation was further increased by the parallel connection (S8_3P) of three semi-solar modules of eight single cells (S8) in series. The increased deviation was attributed to the increased electrical resistances by the extended number of single

cells and contacts. The S8_3P semi-solar modules exhibited faster charging characteristics than the S8 modules because the output current density was higher at the same output voltage. The charging rate constant became almost 10 times higher by the ca. 3-fold increased current density. The present results can contribute to a better understanding of practical applications of organic solar cell modules and the establishment of module design rules.

Acknowledgments: This work was financially supported by the grants from Korean Government (NRF_2015R1A2A2A01003743, NRF_2016H1D5A1910319, 2017M2A2A4A01071010, Basic Science Research Program_2009-0093819).

Author Contributions: Youngkyoo Kim designed this work and supervised whole experimental processes; Myeonghun Song (main), Sooyong Lee, Dohan Kim, Chulyeon Lee, Jaehoon Jeong, and Jooyeok Seo carried out experiments including the measurement system and module structures; Hwajeong Kim was involved in data analysis and discussion; Dong-Ik Song and Donghyun Kim contributed to experimental spaces including miscellaneous supports. Myeonghun Song and Youngkyoo Kim wrote the manuscript and edited the final version.

Conflicts of Interest: The authors declare no conflicts of interest.

References

1. Krebs, F.C. Fabrication and processing of polymer solar cells: A review of printing and coating techniques. *Sol. Energy Mater. Sol. Cells* **2009**, *93*, 394–412. [[CrossRef](#)]
2. Hau, S.K.; Yip, H.-L.; Jen, A.K.-Y. A review on the development of the inverted polymer solar cell architecture. *Polym. Rev.* **2010**, *50*, 474–510. [[CrossRef](#)]
3. Lee, S.; Nam, S.; Seo, J.; Jeong, J.; Kim, H.; Woo, S.; Kim, Y. Polymer solar cells with micrometer-scale engraved active nanolayers fabricated by pressing with metal molds. *Energy Technol.* **2014**, *2*, 713–720. [[CrossRef](#)]
4. Helgesen, M.; Søndergaard, R.; Krebs, F.C. Advanced materials and processes for polymer solar cell devices. *J. Mater. Chem.* **2010**, *20*, 36–60. [[CrossRef](#)]
5. Li, G.; Zhu, R.; Yang, Y. Polymer solar cells. *Nat. Photonics* **2012**, *6*, 153–161. [[CrossRef](#)]
6. Sathiyam, G.; Sivakumar, E.K.T.; Ganesamoorthy, R.; Thangamuthu, R.; Sakthivel, P. Review of carbazole based conjugated molecules for highly efficient organic solar cell application. *Tetrahedron Lett.* **2016**, *57*, 243–252. [[CrossRef](#)]
7. Kim, H.; Nam, S.; Jeong, J.; Lee, S.; Seo, J.; Han, H.; Kim, Y. Organic solar cells based on conjugated polymers: History and recent advances. *Korean J. Chem. Eng.* **2014**, *31*, 1095–1104. [[CrossRef](#)]
8. Krebs, F.C.; Gevorgyan, S.A.; Alstrup, J. A roll-to-roll process to flexible polymer solar cells: Model studies, manufacture and operational stability studies. *J. Mater. Chem.* **2009**, *19*, 5442–5451. [[CrossRef](#)]
9. Krebs, F.C.; Tromholt, T.; Jørgensen, M. Upscaling of polymer solar cell fabrication using full roll-to-roll processing. *Nanoscale* **2010**, *2*, 873–886. [[CrossRef](#)] [[PubMed](#)]
10. Yu, G.; Gao, J.; Hummelen, J.C.; Wudl, F.; Heeger, A.J. Polymer photovoltaic cells: Enhanced efficiencies via a network of internal donor-acceptor heterojunctions. *Science* **1995**, *270*, 1789–1791. [[CrossRef](#)]
11. Halls, J.J.M.; Walsh, C.A.; Greenham, N.C.; Marseglia, E.A.; Friend, R.H.; Moratti, S.C.; Holmes, A.B. Efficient photodiodes from interpenetrating polymer networks. *Nature* **1995**, *376*, 498–500. [[CrossRef](#)]
12. Shaheen, S.E.; Brabec, C.J.; Sariciftci, N.S. 2.5% efficient organic plastic solar cells. *Appl. Phys. Lett.* **2001**, *78*, 841–843. [[CrossRef](#)]
13. Padinger, F.; Rittberger, R.S.; Sariciftci, N.S. Effects of postproduction treatment on plastic solar cells. *Adv. Funct. Mater.* **2003**, *13*, 85–88. [[CrossRef](#)]
14. Kim, Y.; Choulis, S.A.; Nelson, J.; Bradley, D.D.C.; Cook, S.; Durrant, J.R. Composition and annealing effects in polythiophene/fullerene solar cells. *J. Mater. Sci.* **2005**, *40*, 1371–1376. [[CrossRef](#)]
15. Chu, C.-W.; Li, S.-H.; Chen, C.-W.; Shrotriya, V.; Yang, Y. High-performance organic thin-film transistors with metal oxide/metal bilayer electrode. *Appl. Phys. Lett.* **2005**, *87*, 193508. [[CrossRef](#)]
16. Kim, Y.; Choulis, S.A.; Nelson, J.; Bradley, D.D.C. Device annealing effect in organic solar cells with blends of regioregular poly(3-hexylthiophene) and soluble fullerene. *Appl. Phys. Lett.* **2005**, *86*, 063502. [[CrossRef](#)]
17. Li, G.; Shrotriya, V.; Huang, J.; Yao, Y.; Moriarty, T.; Emery, K.; Yang, Y. High-efficiency solution processable polymer photovoltaic cells by self-organization of polymer blends. *Nat. Mater.* **2005**, *4*, 864–868. [[CrossRef](#)]

18. Reyes-Reyes, M.; Kim, K.; Carroll, D.L. High-efficiency photovoltaic devices based on annealed poly(3-hexylthiophene) and 1-(3-hexylthiophene) and 1-(3-methoxycarbonyl)-propyl-1-phenyl-(6,6)C₆₁ blends. *Appl. Phys. Lett.* **2005**, *87*, 083506. [[CrossRef](#)]
19. Kim, Y.; Cook, S.; Tuladhar, S.M.; Choulis, S.A.; Nelson, J.; Durrant, J.R.; Bradley, D.D.C.; Giles, M.; McCulloch, I.; Ha, C.-S.; et al. A strong regioregularity effect in self-organizing conjugated polymer films and high-efficiency polythiophene:fullerene solar cells. *Nat. Mater.* **2006**, *5*, 197–203. [[CrossRef](#)]
20. Park, S.; Nam, S.; Seo, J.; Jeong, J.; Lee, S.; Kim, H.; Kim, Y. Effect of halogen-terminated additives on the performance and the nanostructure of all-polymer solar cells. *J. Korean Phys. Soc.* **2015**, *66*, 521–525. [[CrossRef](#)]
21. Snaith, H.J.; Arias, A.C.; Morteani, A.C.; Silva, C.; Friend, R.H. Charge generation kinetics and transport mechanisms in blended polyfluorene photovoltaic devices. *Nano Lett.* **2002**, *2*, 1353–1357. [[CrossRef](#)]
22. Kim, Y.; Cook, S.; Choulis, S.A.; Nelson, J.; Durrant, J.R.; Bradley, D.D.C. Organic photovoltaic devices based on blends of regioregular poly(3-hexylthiophene) and poly(9,9-dioctylfluorene-co-benzothiadiazole). *Chem. Mater.* **2004**, *16*, 4812–4818. [[CrossRef](#)]
23. Nam, S.; Woo, S.; Seo, J.; Kim, W.H.; Kim, H.; McNeill, C.R.; Shin, T.J.; Bradley, D.D.C.; Kim, Y. Pronounced cosolvent effects in polymer:polymer bulk heterojunction solar cells with sulfur-rich electron-donating and imide-containing electron-accepting polymers. *ACS Appl. Mater. Interfaces* **2015**, *7*, 15995–16002. [[CrossRef](#)] [[PubMed](#)]
24. Zhou, E.; Cong, J.; Wei, Q.; Tajima, K.; Yang, C.; Hashimoto, K. All-polymer solar cells from perylene diimide based copolymers: Material design and phase separation control. *Angew. Chem. Int. Ed.* **2011**, *50*, 2799–2803. [[CrossRef](#)] [[PubMed](#)]
25. Li, S.; Ye, L.; Zhao, W.; Zhang, S.; Ade, H.; Hou, J. Significant influence of the methoxyl substitution position on optoelectronic properties and molecular packing of small-molecule electron acceptors for photovoltaic cells. *Adv. Energy Mater.* **2017**, *7*, 1602000. [[CrossRef](#)]
26. Ye, L.; Xiong, Y.; Yao, H.; Gadisa, A.; Zhang, H.; Li, S.; Ghasemi, M.; Balar, N.; Hunt, A.; O'Connor, B.T.; et al. High performance organic solar cells processed by blade coating in air from a benign food additive solution. *Chem. Mater.* **2016**, *28*, 7451–7458. [[CrossRef](#)]
27. Ye, L.; Xiong, Y.; Li, S.; Ghasemi, M.; Balar, N.; Turner, J.; Gadisa, A.; Hou, J.; O'Connor, B.T.; Ade, H. Precise manipulation of multilength scale morphology and its influence on eco-friendly printed all-polymer solar cells. *Adv. Funct. Mater.* **2017**, *27*, 1702016. [[CrossRef](#)]
28. Nam, S.; Hahm, S.G.; Han, H.; Seo, J.; Kim, C.; Kim, H.; Marder, S.R.; Ree, M.; Kim, Y. All-polymer solar cells with bulk heterojunction films containing electron-accepting triple bond-conjugated perylene diimide polymer. *ACS Sustain. Chem. Eng.* **2016**, *4*, 767–774. [[CrossRef](#)]
29. Fan, B.; Ying, L.; Wang, Z.; He, B.; Jiang, X.-F.; Huang, F.; Cao, Y. Optimisation of processing solvent and molecular weight for the production of green-solvent-processed all-polymer solar cells with a power conversion efficiency over 9%. *Energy Environ. Sci.* **2017**, *10*, 1243–1251. [[CrossRef](#)]
30. Jeong, J.; Seo, J.; Nam, S.; Han, H.; Kim, H.; Anthopoulos, T.D.; Bradley, D.D.C.; Kim, Y. Significant stability enhancement in high-efficiency polymer:fullerene bulk heterojunction solar cells by blocking ultraviolet photons from solar light. *Adv. Sci.* **2016**, *3*, 1500269. [[CrossRef](#)] [[PubMed](#)]
31. Lin, Y.; He, Q.; Zhao, F.; Huo, L.; Mai, J.; Lu, X.; Su, C.-J.; Li, T.; Wang, J.; Zhu, J.; et al. A facile planar fused-ring electron acceptor for as-cast polymer solar cells with 8.71% efficiency. *J. Am. Chem. Soc.* **2016**, *2973–2976*. [[CrossRef](#)] [[PubMed](#)]
32. Nam, S.; Song, M.; Kim, H.; Bradley, D.D.C.; Kim, Y. Thickness effect of bulk heterojunction layers on the performance and stability of polymer:fullerene solar cells with alkylthiophene-containing polymer. *ACS Sustain. Chem. Eng.* **2017**, *5*, 9263–9270. [[CrossRef](#)]
33. Woo, S.; Kim, W.H.; Kim, H.; Yi, Y.; Lyu, H.-K.; Kim, Y. 8.9% single-stack inverted polymer solar cells with electron-rich polymer nanolayer-modified inorganic electron-collecting buffer layers. *Adv. Energy Mater.* **2014**, *4*, 1301692. [[CrossRef](#)]
34. Hwang, Y.J.; Li, H.; Courtright, B.A.E.; Subramaniyan, S.; Jenekhe, S.A. Nonfullerene polymer solar cells with 8.5% efficiency enabled by a new highly twisted electron acceptor dimer. *Adv. Mater.* **2016**, *28*, 124–131. [[CrossRef](#)] [[PubMed](#)]

35. Nam, S.; Seo, J.; Song, M.; Kim, H.; Ree, M.; Gal, Y.-S.; Bradley, D.D.C.; Kim, Y. Polyacetylene-based polyelectrolyte as a universal interfacial layer for efficient inverted polymer solar cells. *Org. Electron.* **2017**, *48*, 61–67. [[CrossRef](#)]
36. Li, S.; Ye, L.; Zhao, W.; Zhang, S.; Mukherjee, S.; Ade, H.; Hou, J. Energy-level modulation of small-molecule electron acceptors to achieve over 12% efficiency in polymer solar cells. *Adv. Mater.* **2016**, *28*, 9423–9429. [[CrossRef](#)] [[PubMed](#)]
37. Bin, H.; Gao, L.; Zhang, Z.-G.; Yang, Y.; Zhang, Y.; Zhang, C.; Chen, S.; Xue, L.; Yang, C.; Xiao, M.; et al. 11.4% efficiency non-fullerene polymer solar cells with trialkylsilyl substituted 2D-conjugated polymer as donor. *Nat. Commun.* **2016**, *7*, 13651. [[CrossRef](#)] [[PubMed](#)]
38. Nam, S.; Seo, J.; Woo, S.; Kim, W.H.; Kim, H.; Bradley, D.D.C.; Kim, Y. Inverted polymer fullerene solar cells exceeding 10% efficiency with poly(2-ethyl-2-oxazoline) nanodots on electron-collecting buffer layers. *Nat. Commun.* **2015**, *6*, 8929. [[CrossRef](#)] [[PubMed](#)]
39. Zhao, W.; Qian, D.; Zhang, S.; Li, S.; Inganäs, O.; Gao, F.; Hou, J. Fullerene-free polymer solar cells with over 11% efficiency and excellent thermal stability. *Adv. Mater.* **2016**, *28*, 4734–4739. [[CrossRef](#)] [[PubMed](#)]
40. Zhao, W.; Li, S.; Yao, H.; Zhang, S.; Zhang, Y.; Yang, B.; Hou, J. Molecular optimization enables over 13% efficiency in organic solar cells. *J. Am. Chem. Soc.* **2017**, *139*, 7148–7151. [[CrossRef](#)] [[PubMed](#)]
41. Ahmed, N.A.; Miyatake, M.; Al-Othman, A.K. Power fluctuations suppression of stand-alone hybrid generation combining solar photovoltaic/wind turbine and fuel cell systems. *Energy Convers. Manag.* **2008**, *49*, 2711–2719. [[CrossRef](#)]
42. Das, D.; Esmaili, R.; Xu, L.; Nichols, D. An optimal design of a grid connected hybrid wind/photovoltaic/fuel cell system for distributed energy production. *Ind. Electron. Soc.* **2005**. [[CrossRef](#)]
43. Gibson, T.L.; Kelly, N.A. Solar photovoltaic charging of lithium-ion batteries. *J. Power Sources* **2010**, *195*, 3928–3932. [[CrossRef](#)]
44. Dennler, G.; Bereznev, S.; Fichou, D.; Holl, K.; Ilic, D.; Koeppe, R.; Krebs, M.; Labouret, A.; Lungenschmied, C.; Marchenko, A.; et al. A self-rechargeable and flexible polymer solar battery. *Sol. Energy* **2007**, *81*, 947–957. [[CrossRef](#)]
45. Schmidt, D.; Hager, M.D.; Schubert, U.S. Photo-rechargeable electric energy storage systems. *Adv. Energy Mater.* **2016**, *6*, 1500369. [[CrossRef](#)]
46. Tanenbaum, D.M.; Dam, H.F.; Rösch, R.; Jørgensen, M.; Hoppe, H.; Krebs, F.C. Edge sealing for low cost stability enhancement of roll-to-roll processed flexible polymer solar cell modules. *Sol. Energy Mater. Sol. Cells* **2012**, *97*, 157–163. [[CrossRef](#)]
47. Kang, N.S.; Ju, B.-K.; Yu, J.-W. Module structure for an organic photovoltaic device. *Sol. Energy Mater. Sol. Cells* **2013**, *116*, 219–223. [[CrossRef](#)]
48. Aernouts, T.; Vanlaeke, P.; Geens, W.; Poortmans, J.; Heremans, P.; Borghs, S.; Mertens, R.; Andriessen, R.; Leenders, L. Printable anodes for flexible organic solar cell modules. *Thin Solid Films* **2004**, *451–452*, 22–25. [[CrossRef](#)]
49. Kim, Y.; Ballantyne, A.M.; Nelson, J.; Bradley, D.D.C. Effects of thickness and thermal annealing of the PEDOT: PSS layer on the performance of polymer solar cells. *Org. Electron.* **2009**, *10*, 205–209. [[CrossRef](#)]

